Quasi-phase-matched spontaneous parametric down-conversion in chiral ferroelectric nematic liquid crystals

Aljaž Kavčič [1,2] Nerea Sebastián [1] and Matjaž Humar [1,2,3,*]
[1] *Jožef Stefan Institute, 1000 Ljubljana, Slovenia*
[2] *Faculty of Mathematics and Physics, University of Ljubljana, 1000 Ljubljana, Slovenia*
[3] *CENN Nanocenter, 1000 Ljubljana, Slovenia*

(Received 21 July 2025; revised 6 November 2025; accepted 16 December 2025; published 2 February 2026)

For high-intensity photon pair generation via spontaneous parametric down-conversion, phase matching or quasi-phase-matching must be realized. The most common method is to use periodically poled crystals, where quasi-phase-matching is achieved through the periodic modulation of the nonlinear susceptibility. In contrast to solid-state materials typically employed, an alternative approach is demonstrated here by using chiral ferroelectric nematic liquid crystals (FNLCs). It involves the spontaneous formation of a twisted periodic arrangement of liquid crystal molecules that depends only on the concentration of chiral dopants. This enables the rapid and scalable fabrication of nonlinear optical media with a tunable periodicity of the structure. We show that within only 20 μm, we can enhance the signal by 2 orders of magnitude compared to the maximal achievable rate for the non-phase-matched case. This process enables us to achieve a significantly enhanced photon pair generation rate of over 1200 Hz/mW in a very short interaction length while simultaneously maintaining a high degree of polarization entanglement. These results establish chiral FNLCs as a versatile, reconfigurable, and low-cost platform for nonlinear and quantum photonics.

DOI: 10.1103/wgb3-clj5

I. INTRODUCTION

Most sources for generating entangled photons rely on spontaneous parametric down-conversion (SPDC) in a nonlinear medium [1,2]. The efficiency of SPDC depends on phase matching between the pump and twin photons [3]. Simply increasing the thickness of nonlinear medium does not improve brightness unless phase matching is maintained. This can be achieved with birefringent media [4], but materials with sufficient birefringence and access to arbitrary nonlinear susceptibility components are limited. An effective solution is quasi-phase-matching via periodic poling [3,5,6], where the crystal axis orientation is periodically flipped. This technique modulates the nonlinear susceptibility rather than the effective refractive index of the input and output beams. Appropriate periodicity neutralizes phase mismatch, and constructive amplification extends to the entire length of the structure [7–10]. Periodically poled devices are the main platform for SPDC generation and related nonlinear technologies, due to their flexibility, removing constraints on birefringence and accessible nonlinear susceptibility components, and enabling high photon pair generation rates.

However, fabricating such structures is complex, requires high-voltage electrode patterning, and primarily only enables assembly of thin domains. Moreover, achieving high poling quality for small poling periods (well below 10 μm)—essential for visible wavelengths—remains challenging [8,9]. These structures also offer very limited thermal tunability [11], restricting them to fixed pump wavelengths, which limits their application in active and tunable quantum devices.

In our recent work [12], we demonstrated SPDC photon pair generation in a very different class of materials—ferroelectric nematic liquid crystals (FNLCs) [13–16]. Due to the broken inversion symmetry and large first molecular hyperpolarizability, FNLCs exhibit high second-order nonlinearities comparable to those of the state-of-the-art solid-state crystals [16–18]. Their fluidity and large response to external stimuli enable tuning of both efficiency and quantum state of the photon pairs, making them a fascinating new platform for quantum optics applications [12].

Due to their periodicity, chiral FNLCs are a promising alternative to periodic poling [19–21]. In chiral nematic liquid crystals [22,23], the orientation of the molecules follows a helical twist described by the pitch p, corresponding to the length of a full 2π rotation. For chiral FNLCs, this also corresponds to the 2π turn of the polarization vector [19,20]. These structures can self-assemble by simply adding a chiral dopant [20], with pitch controlled by its concentration. Enhanced second harmonic generation (SHG) [20,24,25] and preliminary SPDC results [26] have been shown, although phase matching and entanglement were not analyzed in detail.

Here, we demonstrate that by tuning the pitch of chiral FNLCs, quasi-phase-matching is realized, resulting in enhancement of photon pair generation throughout the entire interaction length. Based on ease of production due to self-assembly, even on very large surfaces, and tunable periodicity

*Contact author: matjaz.humar@ijs.si

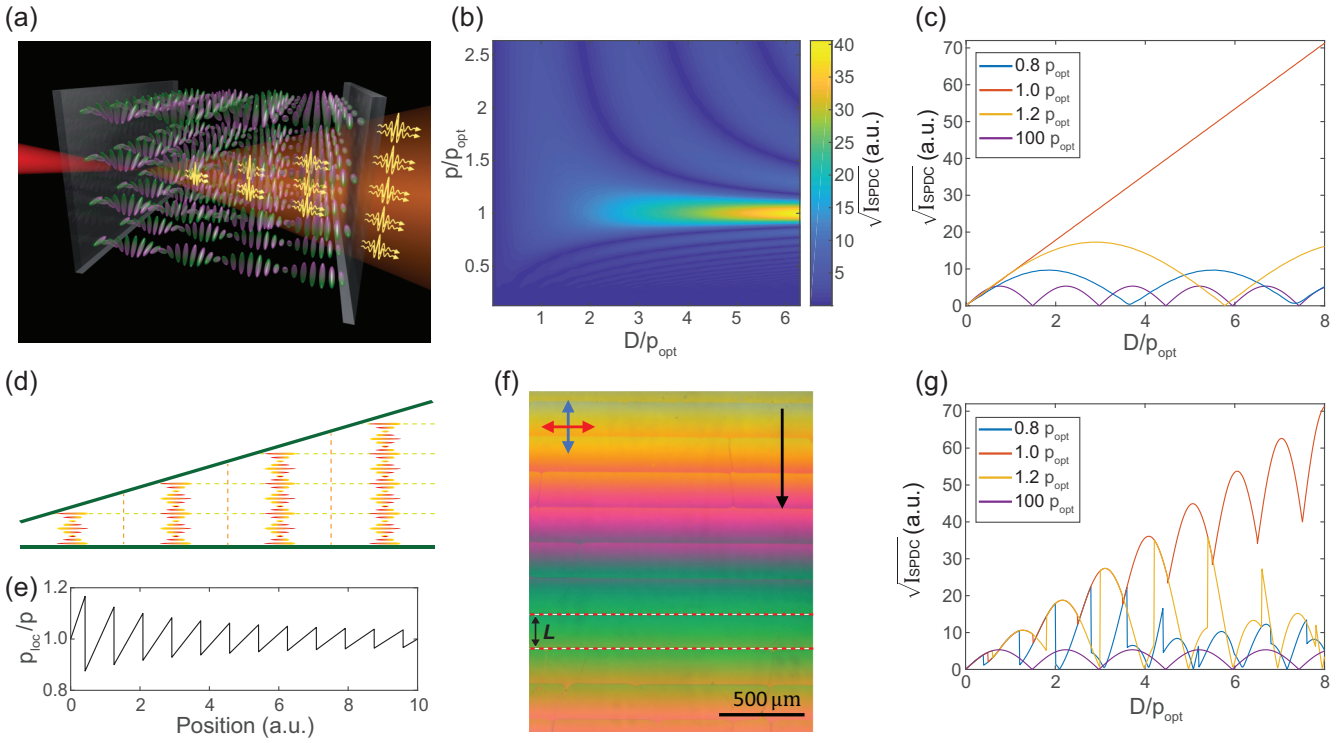

FIG. 1. (a) A chiral FNLC structure with optimal helical pitch amplifies SPDC signal with increasing thickness. (b) Calculated SPDC intensity vs sample thickness (D) and pitch (p), where p_{opt} denotes the optimal pitch yielding maximal amplification. (c) Calculated square root of SPDC intensity vs thickness for four pitches. For $p = p_{\mathrm{opt}}$, the intensity grows quadratically. (d) Wedge cells with linear thickness profile and parallel surface anchoring filled with chiral FNLCs. Vertical lines denote disclination lines. (e) Local pitch p_{loc} varies with thickness and experiences discrete jumps at disclinations. (f) Image of a sample with $p = 1.8\,\mu$m under crossed polarizers in a wedge cell with $\theta = 0.47^{\circ}$, showing birefringence-induced color variation and disclinations separated by distance L. Arrow indicates the direction of thickness increase. (g) Calculated square root of SPDC intensity vs thickness for four pitches from panel (c), considering varying local pitch. Discrete jumps appear at disclination positions.

with changing dopant concentration, results shown here provide additional benefits for FNLCs as an emerging platform for quantum optics.

II. RESULTS

In this study, we utilized a ferroelectric nematic liquid crystal, FNLC-1571 from Merck, along with two of its chiral variations (with pitches of 0.6 and 4.6 µm) that were prepared by adding a proprietary chiral dopant. This FNLC has refractive indices of $n_e = 1.69$ and $n_o = 1.48$ at 600 nm and a single significant component of the second-order nonlinear tensor ($d_{33} \approx 20\,\mathrm{pm/V}$) [12]. By mixing the components with different dopant concentrations, we had access to pitches larger than 0.6 µm. By preparing a sample with just the right pitch, the intensity of SPDC emission is expected to monotonically increase with sample length as schematically represented in Fig. 1(a).

The influence of the pitch on the amplification of SPDC signal with FNLC sample thickness D was calculated based on a theoretical model for calculating the intensity and state of SPDC in twisted FNLC structures devised in our recent paper [12]. We can calculate how the intensity of SPDC depends on the sample thickness for different values of p [Figs. 1(b) and 1(c)]. If the pitch is either too long or too short, the phases do not add up constructively, and after a certain propagation length, the signal begins to decrease. This behavior then repeats in a periodic pattern. The closer the pitch is to the optimal, the longer the period and the larger the increase in intensity. For the optimal pitch length $p = p_{\mathrm{opt}}$, the period diverges and the signal keeps on increasing quadratically with thickness.

To experimentally measure this dependence, we assembled the so-called Grandjean-Cano wedge cells with parallel rubbing [27], where the thickness of the cell linearly increases in one direction [dihedral angles in the range $\theta = 0.046^{\circ}$–0.47°, Fig. 1(d)] and filled them with chiral mixtures with different pitches in the range $p = 1.8$–$4.6\,\mu$m. By measuring the SHG or SPDC intensity at various positions, we can assess the thickness dependence. Due to the surface anchoring, which defines the orientation of the macroscopic polarization P on both surfaces relative to the rubbing direction, the pitch cannot be exactly constant throughout the sample, but has to adjust itself, adopting a local pitch p_{loc}. At certain positions, the equilibrium structure adapts to the change in thickness by introducing a line defect perpendicular to the thickness gradient, at which the number of 2π rotations jumps by 1 [19,20,27]. The estimated local pitch dependence is shown in Fig. 1(e).

The material's cholesteric pitch p can be determined by polarizing optical microscopy [Fig. 1(f)], measuring the

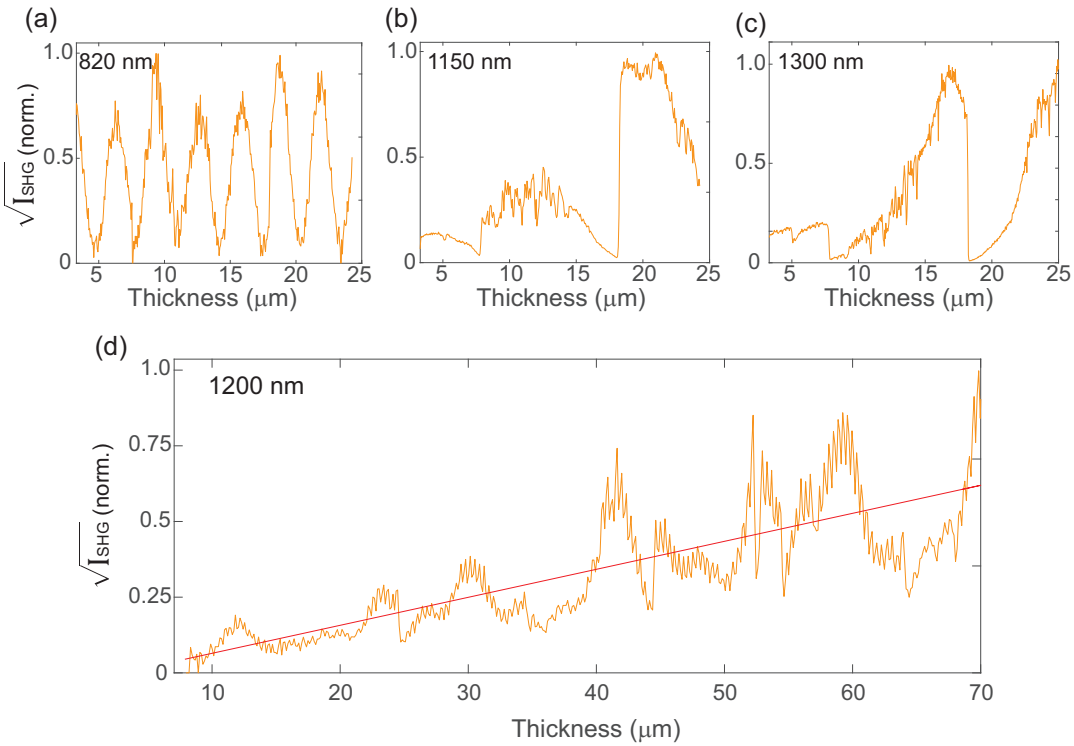

FIG. 2. Square root of SHG intensity vs thickness for a sample with $p = 4.6\,\mu$m, measured with different pump wavelengths. (a) At 820 nm, the system is non-phase-matched and intensity oscillates without net increase. At (b) 1150 nm and (c) 1300 nm, the system is approaching quasi-phase-matching. Shape of discrete jumps, originating from local pitch disclinations, indicates that the optimal wavelength for this pitch lies between these two values. (d) At 1200 nm, quasi-phase-matching is realized and SHG intensity on average grows quadratically with thickness. Across panels, each curve is normalized to its own maximum. Vertical scales are not comparable and only relative trends should be compared.

distance separating the disclinations (L), as $p = L \tan\theta$. In the present context, what is important to consider is that due to this periodic variation in local pitch, the produced signal will not only increase monotonically but will possess positional (thickness) fluctuations. This is demonstrated in the calculations considering a sawlike local pitch profile like shown in Fig. 1(e). The discrete jumps in the signal at the positions of the disclinations are more apparent the closer p is to p_{opt} [Fig. 1(g)]. If the pitch is shorter than optimal, crossing a disclination line results in a discrete decrease in intensity, whereas for pitches longer than optimal, it leads to a discrete increase. This was also observed in the experimental results and is discussed later in the paper.

III. QUASI-PHASE-MATCHED SHG

To estimate the appropriate pitch for SPDC experiments at a given pump wavelength, we first performed SHG measurements with varying pump wavelengths on a sample with $p = 4.6\,\mu$m. As the properties of the material, such as refractive index, birefringence, and coherence length, depend on wavelength, so does the optimal pitch length p_{opt}. By finding the pump wavelength at which the SHG amplification is the most pronounced, we can reverse calculate which pitch would give similar amplification at a different pump wavelength. As changing the wavelength is much faster, as well as more precise and well defined than changing the pitch, this gives the optimal way to design the right sample properties.

A tunable nanosecond OPO laser with a broad wavelength range 400–2400 nm, pulse energy of 100 μJ, and 20 Hz repetition rate was used as the pump for SHG. The produced SHG signal was collected with a spectrometer with a 10 μm wide slit and a CCD detector with a resolution of 1600 × 200 pixels. With this configuration, the SHG signal could be easily distinguished from the unwanted background.

The results for four different pump wavelengths are presented in Fig. 2. For 820 nm laser [Fig. 2(a)], the signal shows periodic modulation in intensity as in a typical non-phase-matched case. For 1150 nm [Fig. 2(b)], the intensity reaches much higher values, the period of modulation is greatly enhanced, and the amplitudes of successive maxima are increasingly higher. However, the signal still decreases to zero at certain thicknesses. For thicknesses larger than the range presented here, the maxima would start to decrease again. Similar behavior can also be observed for 1300 nm [Fig. 2(c)]. Discrete periodic jumps in the produced signal are present, corresponding to the positions of the disclinations (discrete jumps in local pitch). For 1150 nm they manifest as increases, while for 1300 nm as decreases in intensity. This opposing behavior indicates that 1150 nm is too short, while 1300 nm is too long, indicating that the optimal pump wavelength at this pitch lies somewhere in between. Indeed, we confirm that we can achieve a quasi-phase-matched regime at 1200 nm [Fig. 2(d)]. Disregarding the fluctuations caused by variations in local pitch, the signal exhibits an overall quadratic increase. With this, a quasi-phase-matched regime

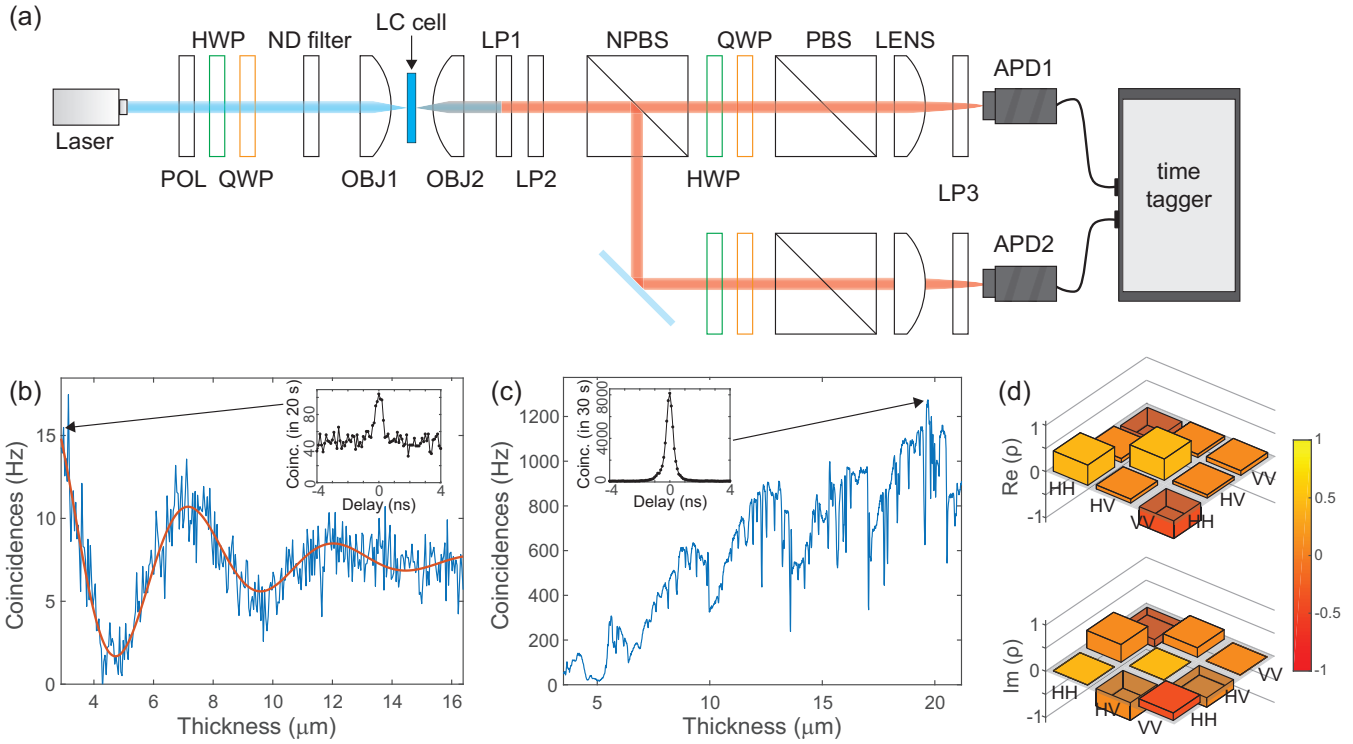

FIG. 3. (a) Schematic illustration of experimental setup for generation and detection of SPDC photon pairs. POL, linear polarizer; HWP, half-wave plate; QWP, quarter-wave plate; ND filter, neutral density filter; OBJ, objective; LP, long-pass filter; (N)PBS, (non)polarizing beam splitter; APD, avalanche photodiode detector. The wave plates and PBS in each arm are used only for tomography. (b) SPDC coincidence rate vs thickness for a nonchiral FNLC shows oscillatory behavior without net increase. Red line shows a damped sine fit. Inset: Coincidence histogram at $D = 2.9\,\mu$m. (c) SPDC coincidence rate vs thickness for a chiral FNLC with $p = 3.7\,\mu$m shows steady amplification, reaching intensities 100× higher than in the nonchiral FNLC. Inset: Coincidence histogram at $D = 19.7\,\mu$m. (d) Real (top) and imaginary part (bottom) of the reconstructed polarization state density matrix.

has been found by tuning the pump wavelength. Since quasi-phase-matching works similarly for both SGH and SPDC, these results are transferable to SPDC.

IV. QUASI-PHASE-MATCHED SPDC

To measure SPDC, samples were pumped with a 450 nm continuous-wave laser with 1 mW power, which was linearly polarized in the same direction as the direction of the sample surface anchoring. The reason for choosing this polarization is that the only significant component of the nonlinear tensor (d_{33}) will be maximally utilized when the pump polarization coincides with the molecule's axis. The signal was collected by two single-photon avalanche photodiodes arranged in a Hanbury-Brown and Twiss configuration, allowing us to examine the correlations between the arrival times of the generated photons [Fig. 3(a)]. SPDC-produced photons arrive at the detectors simultaneously and therefore create a coincidence peak in the distribution of time delays between successive detections [insets in Figs. 3(b) and 3(c)]. The area below the coincidence peak determines the intensity of the SPDC signal. The spectral properties of photon pairs in this material were characterized in our previous study [12], revealing a broadband two-photon spectrum indicating strong time-frequency entanglement. Nevertheless, like in conventional periodically polled crystals, we expect narrowing of the spectrum with increasing material thickness. Additional spectral metrics will be measured in future with a dedicated setup designed for high-fidelity spectral reconstruction.

First, we considered an undoped sample where there is no chiral structure and the molecular orientation remains constant throughout the entire sample thickness. In this case, the intensity periodically varies with thickness, as there is no mechanism to compensate for the phase mismatch between pump and twin photons [Fig. 3(b)]. The apparent dampening of the amplitude of the oscillations was attributed to the fact that the photons are generated with a broad angular spectrum even from a collimated pump beam due to the freedom of the twin-photon emission wavelength and lack of phase matching. This feature cannot be mitigated by tailoring the pump properties. Photons with a smaller angle have shorter propagation lengths, while photons emitted at a larger angle have longer propagation lengths through the material. For a thin sample, these differences are small, but for thicker ones, they become significant and lead to averaging out of any phase difference effects.

Next, we focused on different chiral mixtures. We have prepared samples with different pitches ranging from 1.8 to 4.6 μm and measured their SPDC intensity versus thickness. We were able to confirm the observations from simulations and SHG measurements that the discrete periodic jumps

in the produced signal are present, with a decrease in intensity for too short and an increase in intensity for too long p.

The samples with $p = 3.7\,\mu$m generated the most coincidences. This pitch was beforehand estimated to be close to p_{opt} according to SHG measurements with varying pump wavelength. The appropriate pitch overcomes the lack of phase matching and results in a signal that drastically increases with thickness, as shown in Fig. 3(c). This demonstrates a clear distinction between nonchiral and chiral FNLC samples in terms of SPDC generation intensity. We can see that the maximal generation rate of the sample without the chiral structure is 15 photon pairs per second, while a chiral structure with $p = 3.7\,\mu$m produces over 1200 photon pairs per second at a thickness of $20\,\mu$m. At larger thicknesses, some of the results exhibit significant variability, visible primarily as sudden dips in intensity, which originate from defects in the sample. The defects are formed both between the domains with a different number of full rotations and within domains in the form of the well-known oily streaks [28]. Mitigation of defects is achievable through improved sample fabrication, such as optimizing the cooling rate, better surface alignment, applying small voltage during preparation, and switching from wedge to uniform cells. Future work will focus on optimizing these steps to enhance uniformity, reproducibility, and overall sample quality. Since p is not completely optimal, we did not achieve a quadratic increase in the signal with increasing thickness; however, this is certainly possible, as we demonstrated for SHG, where we could tune the pump wavelength. While typical bulk PPKTP and PPLN sources yield higher detection rates of 10^4–10^6 pairs/(s mW) [29–31], this is achieved with much longer crystals. Taking into account the interaction length, we achieve 6×10^4 pairs/(s mW mm), while solid-state periodically poled crystals typically generate $0.5-4 \times 10^4$ pairs/(s mW mm). This already makes our source completely competitive with the best periodically poled crystals, while greatly surpassing them in terms of tunability and control. With more homogeneous samples and further optimizations of the pitch, as well as an optimized detection system, we expect further significant enhancement.

Additionally, to assess the photon pair polarization state, we performed polarization tomography [32] through which the two-photon wave function and its corresponding density matrix [33] can be reproduced [Fig. 3(d)]. In the case where two photons are distinguishable in no other way than polarization, symmetry restrictions reduce the number of independent basis states to 3 as only the photon-number occupation of each polarization mode matters. The resulting state is a qutrit—a superposition of vertically, horizontally, and orthogonally polarized photon-pair Fock states [34,35]:

$$|\psi\rangle = c_1\,|2_H 0_V\rangle + c_2\,|1_H 1_V\rangle + c_3\,|0_H 2_V\rangle\,.$$

With multiple components of the density matrix occupied, the results demonstrate that the state is not trivial with the calculated degree of polarization entanglement 0.75 ± 0.03, quantified with concurrence $C = |2c_1c_3 - c_2^2|$ [36–38]. The state is reproducible across the entire sample with less than 5% variations at different positions and thicknesses. Only within the first domain, the fluctuations are higher due to large differences in the local pitch, but we are mainly interested in the state at large thicknesses with high rates of photon pairs. As high entanglement is desired for the majority of quantum applications, this result is very promising. Due to the high tunability of FNLCs, it is highly probable that even greater degree of entanglement could be achieved in the future.

V. DISCUSSION

We have demonstrated an approach for quasi-phase-matched SPDC using spontaneously formed chiral structures in FNLCs. This self-assembled periodic modulation of the nonlinear susceptibility enables compensation for phase mismatch and significant amplification of the SPDC signal over short propagation distances. In contrast to conventional periodically poled crystals, our method relies solely on tuning the concentration of a chiral dopant, allowing for rapid, low-cost, and scalable fabrication. While further refinement is needed—such as further optimizing the pitch, minimizing structural defects, and enabling thicker, defect-free samples—these challenges are surmountable with improved sample preparation.

Chiral FNLCs show robust long-term and environmental stability, with the pitch—and thus the quasi-phase-matching condition—remaining stable over time. Specifically, we have not observed any structural changes or variations in the measured SHG and SPDC signals in the investigated samples over a period of approximately one month of constant operation. The FNLC material used here operates from below room temperature up to approximately 46 °C, while materials with an even larger operating range are being developed. Further, the refractive indices and the pitch of FNLCs show minimal variation with temperature [21,39], significantly smaller than for regular cholesteric LCs. Their structure can also be dynamically controlled via electric fields [40,41]. Such mechanisms could enable broad real-time tuning of quasi-phase-matching conditions, well beyond what is currently achievable in solid-state materials. With their strong second-order nonlinearity, intrinsic fluidity, self-assembly, and external tunability, FNLCs provide a compelling and reconfigurable platform for quantum and nonlinear photonic applications.

ACKNOWLEDGMENTS

The authors thank Merck Electronics KGaA for providing the FNLC material and Janja Milivojević for assembling LC cells. This project has received funding from the Slovenian Research and Innovation Agency (ARIS) (P1-0099 and P1-0192). This work is supported by ERC Grant (SoftQuanta, 101170123).

A.K. performed the experimental work, theoretical simulations, and analysis of the results. N.S. helped with sample preparation. A.K. and M.H. wrote the manuscript. All authors approved the final version of the paper.

DATA AVAILABILITY

The data that support the findings of this article are openly available [42]; embargo periods may apply.

[1] C. Couteau, Spontaneous parametric down-conversion, Contemp. Phys. **59**, 291 (2018).

[2] P. G. Kwiat, K. Mattle, H. Weinfurter, A. Zeilinger, A. V. Sergienko, and Y. Shih, New high-intensity source of polarization-entangled photon pairs, Phys. Rev. Lett. **75**, 4337 (1995).

[3] R. W. Boyd, A. L. Gaeta, and E. Giese, Nonlinear optics, in *Springer Handbook of Atomic, Molecular, and Optical Physics*, editrd by W. F. D. Gordon (Springer, Cham, 2008), pp. 1097–1110.

[4] A. Burlakov, M. Chekhova, O. Karabutova, and S. Kulik, Collinear two-photon state with spectral properties of type-I and polarization properties of type-II spontaneous parametric down-conversion: Preparation and testing, Phys. Rev. A **64**, 041803 (2001).

[5] R. L. Byer, Quasi-phase-matched nonlinear interactions and devices, J. Nonlinear Opt. Phys. Mater. **6**, 549 (1997).

[6] K. L. Vodopyanov *et al.*, Optical parametric oscillation in quasi-phase-matched GaAs, Opt. Lett. **29**, 1912 (2004).

[7] L. Gordon *et al.*, Diffusion-bonded stacked GaAs for quasi-phase-matched second-harmonic generation of a carbon dioxide laser, Electron. Lett. **29**, 1942 (1993).

[8] L. E. Myers *et al.*, Quasi-phase-matched optical parametric oscillators in bulk periodically poled $LiNbO_3$, J. Opt. Soc. Am. B **12**, 2102 (1995).

[9] G. D. Miller, *Periodically Poled Lithium Niobate: Modeling, Fabrication, and Nonlinear Optical Performance* (Stanford University, Stanford, California, USA, 1998).

[10] S. Tanzilli *et al.*, Highly efficient photon-pair source using periodically poled lithium niobate waveguide, Electron. Lett. **37**, 26 (2001).

[11] G. Tawy *et al.*, Temperature-tunable UV generation using an Alexandrite laser and PPLN waveguides, Opt. Express **31**, 22757 (2023).

[12] V. Sultanov *et al.*, Tunable entangled photon-pair generation in a liquid crystal, Nature (London) **631**, 294 (2024).

[13] H. Nishikawa *et al.*, A fluid liquid-crystal material with highly polar order, Adv. Mater. **29**, 1702354 (2017).

[14] R. J. Mandle, S. J. Cowling, and J. W. Goodby, A nematic to nematic transformation exhibited by a rod-like liquid crystal, Phys. Chem. Chem. Phys. **19**, 11429 (2017).

[15] X. Chen *et al.*, First-principles experimental demonstration of ferroelectricity in a thermotropic nematic liquid crystal: Polar domains and striking electro-optics, Proc. Natl. Acad. Sci. USA **117**, 14021 (2020).

[16] N. Sebastián, L. Cmok, R. J. Mandle, M. R. delaFuente, I. DrevensekOlenik, M. Copic, and A. Mertelj, Ferroelectric-ferroelastic phase transition in a nematic liquid crystal, Phys. Rev. Lett. **124**, 037801 (2020).

[17] N. Sebastián, R. J. Mandle, A. Petelin, A. Eremin, and A. Mertelj, Electrooptics of mm-scale polar domains in the ferroelectric nematic phase, Liq. Cryst. **48**, 2055 (2021).

[18] C. L. Folcia, J. Ortega, R. Vidal, T. Sierra, and J. Etxebarria, The ferroelectric nematic phase: An optimum liquid crystal candidate for nonlinear optics, Liq. Cryst. **49**, 899 (2022).

[19] H. Nishikawa and F. Araoka, A new class of chiral nematic phase with helical polar order, Adv. Mater. **33**, 2101305 (2021).

[20] X. Zhao *et al.*, Spontaneous helielectric nematic liquid crystals: Electric analog to helimagnets, Proc. Natl. Acad. Sci. USA **118**, e2111101118 (2021).

[21] C. Feng *et al.*, Electrically tunable reflection color of chiral ferroelectric nematic liquid crystals, Adv. Opt. Mater. **9**, 2101230 (2021).

[22] P.-G. De Gennes and J. Prost, *The Physics of Liquid Crystals* (Oxford University Press, Oxford, 1993).

[23] C. Bahr and H.-S. Kitzerow, *Chirality in Liquid Crystals* (Springer, New York, 2001).

[24] X. Zhao *et al.*, Nontrivial phase matching in helielectric polarization helices: Universal phase matching theory, validation, and electric switching, Proc. Natl. Acad. Sci. USA **119**, e2205636119 (2022).

[25] X. Zhao, J. Li, M. Huang, and S. Aya, High-*g*-factor phase-matched circular dichroism of second harmonic generation in chiral polar liquids, J. Mater. Chem. C **11**, 8547 (2023).

[26] J.-T. Pan *et al.*, Nonreciprocal quantum photon-pair source with chiral ferroelectric nematics, arXiv:2503.11399.

[27] K. Thapa *et al.*, Confinement and magnetic-field effect on chiral ferroelectric nematic liquid crystals in Grandjean-Cano wedge cells, Phys. Rev. E **109**, 054702 (2024).

[28] O. Lavrentovich and D.-K. Yang, Cholesteric cellular patterns with electric-field-controlled line tension, Phys. Rev. E **57**, R6269 (1998).

[29] M. Bock, A. Lenhard, C. Chunnilall, and C. Becher, Highly efficient heralded single-photon source for telecom wavelengths based on a PPLN waveguide, Opt. Express **24**, 23992 (2016).

[30] F. Steinlechner *et al.*, A high-brightness source of polarization-entangled photons optimized for applications in free space, Opt. Express **20**, 9640 (2012).

[31] Omshankar, V. Venkataraman, and J. Ghosh, Bright source of narrowband polarization-entangled photons from a thick type-II ppKTP crystal, Opt. Express **32**, 3470 (2024).

[32] A. Burlakov, L. Krivitskii, S. Kulik, G. Maslennikov, and M. Chekhova, Measurement of qutrits, Opt. Spectrosc. **94**, 684 (2003).

[33] C. C. Gerry and P. L. Knight, *Introductory Quantum Optics* (Cambridge University Press, Cambridge, UK, 2023).

[34] A. Burlakov, M. Chekhova, O. Karabutova, D. Klyshko, and S. Kulik, Polarization state of a biphoton: Quantum ternary logic, Phys. Rev. A **60**, R4209 (1999).

[35] A. Burlakov and D. Klyshko, Polarized biphotons as "optical quarks", J. Exp. Theor. Phys. Lett. **69**, 839 (1999).

[36] V. Sultanov, T. Santiago-Cruz, and M. V. Chekhova, Flat-optics generation of broadband photon pairs with tunable polarization entanglement, Opt. Lett. **47**, 3872 (2022).

[37] M. Fedorov, P. Volkov, J. M. Mikhailova, S. Straupe, and S. Kulik, Entanglement of biphoton states: Qutrits and ququarts, New J. Phys. **13**, 083004 (2011).

[38] M. Fedorov and N. Miklin, Schmidt modes and entanglement, Contemp. Phys. **55**, 94 (2014).

[39] J. Karcz *et al.*, Spontaneous chiral symmetry breaking in polar fluid–heliconical ferroelectric nematic phase, Science **384**, 1096 (2024).

[40] M. S. H. Himel *et al.*, Electrically tunable chiral ferroelectric nematic liquid crystal reflectors, Adv. Funct. Mater. **35**, 2413674 (2025).

[41] J. Ortega, C. L. Folcia, J. Etxebarria, and T. Sierra, Ferroelectric chiral nematic liquid crystals: New photonic materials with multiple bandgaps controllable by low electric fields, Liq. Cryst. **49**, 2128 (2022).

[42] M. Humar, A. Kavčič, and N. Sebastian, Data for SPDC in FNLC, Zenodo (2025), doi:http://doi.org/10.5281/zenodo.16263027.